Magneto-optical conductivity in a topological insulator

Zhou Li[1,*] and J. P. Carbotte[1,2,†]

[1]*Department of Physics, McMaster University, Hamilton, Ontario L8S 4M1, Canada*

[2]*Canadian Institute for Advanced Research, Toronto, Ontario M5G 1Z8, Canada*

(Received 22 May 2013; published 8 July 2013)

Adding a small subdominant quadratic-in-momentum term to a dominant linear Dirac dispersion curve affects conduction and valence band differently and leads to an hourglass-like structure for energy as a function of momentum. This applies to the protected surface states in topological insulators. The energies of the conduction and valence band Landau levels are also different and this leads to the splitting of optical absorption lines produced by the magnetic field, which acquire a two-peak structure. It also changes the peaks in the imaginary part of the Hall conductivity into two distinct contributions of opposite signs. The real part of the circularly polarized optical conductivity, however, retains its single-peak structure but the peaks in right and left handedness cases are shifted in energy with respect to each other in contrast to the pure Dirac case. The magnitude of the semiclassical cyclotron frequency is significantly modified by the presence of a mass term, as is its variation with value of the chemical potential μ. Its optical spectral weight is found to decrease with increasing μ rather than increase as it does in the pure Dirac limit.

DOI: 10.1103/PhysRevB.88.045414 PACS number(s): 78.20.Ls, 71.70.Di, 73.25.+i

I. INTRODUCTION

Topological insulators are insulating[1–4] in their bulk but have protected metallic surface states which support helical Dirac fermions at the Γ point of the honeycomb lattice surface Brillouin zone. The direction of the in-plane electron spin is locked to be perpendicular to its momentum with opposite spin winding in conduction and valence bands,[5–7] as was confirmed by spin polarized angular resolved photoemission spectroscopy (ARPES). In contrast to the case of graphene where the Dirac cones are nearly symmetric between conduction and valence bands, topological insulators rather exhibit an hourglass shape[5–10] with the valence band fanning out and merging with the bulk valence band. To get the Fermi level to lie in the surface states between the bottom of the bulk conduction band and the top of the bulk valence band requires care, but this can be done by doping. For example one can dope with Sn in $(Bi_{1-\delta}Sn_\delta)_2Te_3$ (see Ref. 4) or Ca in $Bi_{2-\delta}Ca_\delta Se_3$.[5] The dynamics of charge carriers can be probed by optics. The real part of the complex frequency-dependent longitudinal optical conductivity $\sigma(\omega)$ gives the absorption as a function of photon energy. When applied to graphene, good agreement is found between theory and experiment.[11–17] The technique has also been applied to get information on the surface states of topological insulators[9] and other single-layered materials such as MoS_2[18,19] and silicene.[20] Additional valuable information results when a magnetic field is applied. This creates Landau levels (LL), and incident photons can induce transition between these levels.[21–25] Recently it has been applied to the topological insulator $Bi_{0.91}Sb_{0.09}$.[26] In this paper we consider in detail the magneto-optical conductivity of a topological insulator with particular emphasis on the hourglass shape of the Dirac cones. This comes from a quadratic-in-momentum[27] piece in the electron dispersion, and is additional to the usual Dirac part which gives a contribution to the energy linear in momentum. It is well known that a quadratic alone gives LL spacings proportional to the magnetic field B while the linear piece alone gives spacings which are drastically different, going instead as the square root of B. This has important implications for the optical absorption when both parts are present in the fermion dispersion curves as we will find here.

In Sec. II we specify our Hamiltonian and provide solutions for the energy eigenvalues and eigenfunctions under magnetic field. In Sec. III we introduce the formal expressions needed to compute the magneto-conductivity and provide numerical results. Section IV deals with the semiclassical limit when the chemical potential is much larger than the Landau level spacing. Conclusions and a summary are found in Sec. V.

II. SOME FORMALISM

We begin with the Hamiltonian for fermions on the surface of a topological insulator of the form

$$H_0 = \frac{\hbar^2 k^2}{2m} + \hbar v_F(k_x\sigma_y - k_y\sigma_x), \tag{1}$$

where the first term gives the kinetic energy of a fermion of mass m with a dispersion curve that is quadratic (Schrödinger) in momentum (k), and the second piece is a term which describes relativistic Dirac fermions with velocity v_F. In Eq. (1) σ_x and σ_y are Pauli spin matrices. In a magnetic field B oriented perpendicular to the plane of the fermion motion the Hamiltonian becomes

$$H_0 = \frac{\hbar^2|-i\nabla + e\mathbf{A}/\hbar|^2}{2m} + \alpha[(-i\partial_x + eA_x/\hbar)\sigma_y - (-i\partial_y + eA_y/\hbar)\sigma_x], \tag{2}$$

where $\alpha = \hbar v_F$ and $\mathbf{A}$ is the vector potential. In the Landau gauge $\mathbf{A} \equiv (\mathbf{0}, B\hat{x})$, and we get

$$H_0 = \frac{\hbar^2[(-i\partial_x)^2 + (-i\partial_y + eB\hat{x}/\hbar)^2]}{2m} + \alpha[(-i\partial_x)\sigma_y - (-i\partial_y + eB\hat{x}/\hbar)\sigma_x]. \tag{3}$$

Raising and lowering operators

$$a^\dagger = l_B/\sqrt{2}\left[-\partial_x + (x+x_0)/l_B^2\right], \quad a = l_B/\sqrt{2}\left[\partial_x + (x+x_0)/l_B^2\right] \tag{4}$$

with the magnetic length $l_B = 1/\sqrt{e|B|/\hbar}$ and $x_0 = k_y l_B^2$ can be used to reduce Eq. (3) to the form

$$H_0 = \frac{\hbar^2[a^\dagger a + 1/2]}{ml_B^2} - \sqrt{2}\alpha/l_B \begin{bmatrix} 0 & a \\ a^\dagger & 0 \end{bmatrix}. \tag{5}$$

If a Zeeman splitting term (Δ) is added, the Hamiltonian of interest becomes

$$H_0 = \begin{bmatrix} \hbar^2[a^\dagger a + 1/2]/ml_B^2 + \Delta & (\sqrt{2}\alpha/l_B)a \\ (\sqrt{2}\alpha/l_B)a^\dagger & \hbar^2[a^\dagger a + 1/2]/ml_B^2 - \Delta \end{bmatrix} \tag{6}$$

The eigenstates of Eq. (6) are a mixture of the spin-up $(N-1)$th Landau level ($|N-1\rangle_\uparrow$) and spin-down Nth Landau level ($|N\rangle_\downarrow$), which we denote by

$$|N,s\rangle = \begin{bmatrix} C_{\uparrow,N,s}|N-1\rangle_\uparrow \\ C_{\downarrow,N,s}|N\rangle_\downarrow \end{bmatrix}$$

with $s = +/-$ corresponding to positive/negative energy states. The eigenenergies are

$$E_{N,s} = \hbar^2 N/\left(ml_B^2\right) + s\sqrt{\left[\hbar^2/\left(2ml_B^2\right)\right]^2 + 2N\alpha^2/l_B^2}. \tag{7}$$

For $N > 0$ and for $N = 0$

$$E_{N=0} = \hbar^2/\left(2ml_B^2\right), \tag{8}$$

where for simplicity we have set the Zeeman splitting to zero. The corresponding eigenfunctions are obtained from the solutions of the equation

$$\left(-E_0/2 - s\sqrt{E_0^2/4 + 2NE_1^2}\right)C_{\uparrow,N,s} + \sqrt{2NE_1^2}C_{\downarrow,N,s} = 0, \tag{9}$$

where we have introduced the shorthand notation $E_0 = \hbar e|B|/(m)$ and $E_1 = \frac{\alpha}{l_B}$ which refer respectively to the kinetic energy part that originates from the quadratic part (Schrödinger) and the linear (Dirac) part of the original Hamiltonian [Eq. (1)]. We can introduce a measure of "Diracness" P as the ratio E_1^2/E_0^2. When $P \to \infty$ the system is pure Dirac, and as P decreases the system acquires more and more of a Schrödinger character. For $N > 0$ the solution of Eq. (9) is

$$C_{\uparrow,N,s} = \frac{\sqrt{\sqrt{1/4 + 2NP} - s/2}}{J}, \quad C_{\downarrow,N,s} = \frac{s\sqrt{\sqrt{1/4 + 2NP} + s/2}}{J} \tag{10}$$

with $J = \sqrt{2\sqrt{1/4 + 2NP}}$. For the special case $N = 0$, $C_{\uparrow,0} = 0$ and $C_{\downarrow,0} = 1$ and only $s = +$ need be considered. It is interesting to make an estimate of P for specific topological insulators. Following the work in Ref. 28 we obtain for Bi_2Te_3 $m\alpha^2/2\hbar^2 = 0.048$ eV and $eBv_F^2\hbar = 1.2 \times 10^{-4}$ (eV)^2 for a magnetic field of 1 T and for Bi_2Se_3 we get 0.115 eV and 1.6×10^{-4} (eV)^2 respectively. In terms of the bare electron mass m_e we have $m/m_e = 0.09$ and 0.16 for Bi_2Te_3 and Bi_2Se_3 respectively. For Bi_2Te_3 the "Diracness" parameter $P = 74.2$ for an external magnetic field of 1 T. The energy $E_{N,s} \cong E_1\{N/\sqrt{P} + s\sqrt{2N}\}$ $(N \neq 0)$ with the first term representative of the leading contribution to the energy coming from the quadratic piece of the Hamiltonian and the second term comes from the Dirac piece. The Schrödinger piece provides an 8% correction for $N = 1$ $(s = 1)$ while this rises to 26% for $N = 10$. Because P goes like the inverse of B, for $B = 40$ T $P = 1.86$ and the correction to the $N = 1$ case becomes 52%.

The matrix Green's function associated with our Hamiltonian is given by

$$\hat{G}_0(N,i\omega_n) = \frac{1}{2}\sum_{s=\pm}(1 + s\mathbf{F_k}\cdot\sigma)G_0(N,s,i\omega_n) \tag{11}$$

with

$$\mathbf{F_k} = \frac{(\sqrt{2N}E_1, 0, -E_0/2)}{\sqrt{E_0^2/4 + (\sqrt{2N}E_1)^2}} \tag{12}$$

and

$$G_0(N,s,i\omega_n \to \omega + i\delta) = \frac{1}{\omega + \mu - NE_0 - s\sqrt{E_0^2/4 + (\sqrt{2N}E_1)^2} + i\delta} \tag{13}$$

from which we can compute the density of states $D(\omega)$ given by

$$D(\omega) = \frac{-1}{\pi}\frac{1}{2\pi l_B^2}\left[\sum_{N=1,s=\pm} \mathrm{Im}\, G_0(N,s,\omega) + \mathrm{Im}\, G_0(0,+,\omega)\right]. \tag{14}$$

Without a magnetic field we would get

$$D(\omega, B=0) = \frac{-1}{\pi}\frac{1}{2\pi}\int_0^{k_{\mathrm{cut}}} k\,dk \sum_{s=\pm} \mathrm{Im}\, G_0(k,s,\omega) \tag{15}$$

with

$$G_0(k,s,\omega) = \frac{1}{\omega + \mu - \hbar^2k^2/(2m) - s\alpha k + i\delta}, \tag{16}$$

and μ in Eqs. (13) and (16) is the chemical potential where the momentum cutoff is taken as $k_{\mathrm{cut}} = \frac{\alpha m}{\hbar^2}$. Figure 1 is a schematic of the fermion dispersion relation in our model displaying the two-dimensional (2D) Brillouin zone (BZ) of the surface states and the hourglass structure with Dirac point at the Γ point in the BZ. Figure 2 gives results for the density of states $D(\omega)$ as a function of energy $\hbar\omega$ in eV. The top frame contains a quadratic contribution with $m = 0.09m_e$ (our estimate for Bi_2Te_3) while the bottom frame which is included for comparison has $m = \infty$, i.e. represents the pure relativistic Dirac limit. In both cases the magnetic field was set to 1 Tesla in the red dotted curve which is to be compared with the continuous black curve for $B = 0$. Comparing first the black curves in top and bottom frame we see that including the quadratic part in the Hamiltonian [Eq. (1)] has a drastic effect on the density of states. For pure Dirac there is particle-hole symmetry about the Dirac point at $\omega = 0$, while this no longer

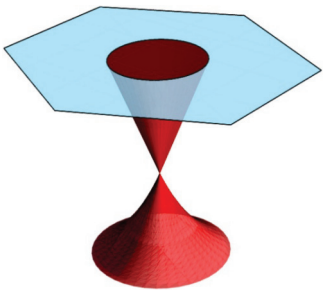

FIG. 1. (Color online) Schematic of Dirac cone centered about the Γ point of the honeycomb Brillouin zone of the surface states in a topological insulator. The top cone is the conduction band while the bottom cone which gives the figure a goblet or hourglass shape is for the valence band.

is the case in the top frame. Both positive and negative energy regions are changed, with the largest difference seen in the negative energy region. This results directly from the hourglass nature of the dispersion curves seen in the schematic of Fig. 1. This change in geometry of the dispersion curves also has a direct effect on the oscillations seen in the red dotted curves. The difference between top and bottom frame are particularly large at negative energies as the large peak around 0.05 eV in the $B = 0$ density of states is sampled. But there are also very significant changes at positive energies both in the position of the peaks and in their amplitude. While in the lower frame (pure Dirac) the red dotted curve around $\hbar\omega = 0.08$ eV has nearly merged with the solid black curve for $B = 0$, this is not the case in the upper curve where the amplitude of the Landau level oscillations remains very significant.

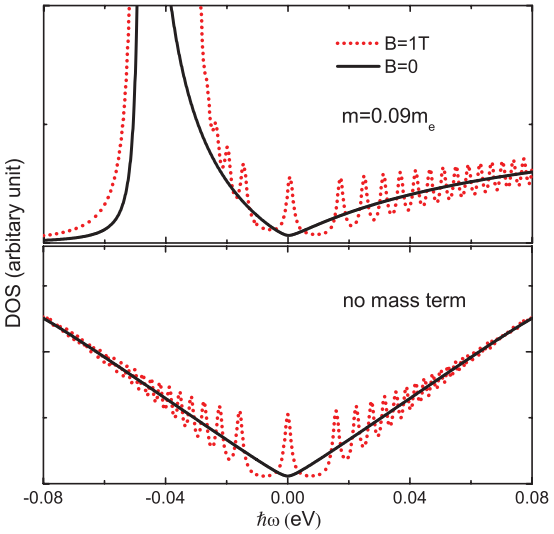

FIG. 2. (Color online) The density of states as a function of energy $\hbar\omega$ in eV for a topological insulator with mass $m = 0.09m_e$ (top frame) and no mass term ($m = \infty$) (bottom frame) shown for comparison. The magnetic field $B = 1$ T. The dotted red curves include B while the solid black are the case of no magnetic field ($B = 0$) included for comparison. The parameters are for Bi_2Te_3, $m = 0.09m_e$ and $\alpha/\hbar = 4.3 \times 10^5$ m/s.

III. MAGNETO-OPTICAL CONDUCTIVITY

The magneto-optical conductivity $\sigma_{\alpha\beta}(\omega)$ based on a system of Landau levels in the clean limit is given by the standard formula

$$\sigma_{\alpha\beta}(\omega) = \frac{-i}{2\pi l_B^2} \sum_{N,N',s,s'} \frac{f_{N,s} - f_{N',s'}}{E_{N,s} - E_{N',s'}} \frac{\langle N,s|j_\alpha|N',s'\rangle\langle N',s'|j_\beta|N,s\rangle}{\omega - E_{N,s} + E_{N',s'} + i/(2\tau)}, \tag{17}$$

where the current operator j_α is related to velocity v_α and

$$\begin{aligned} v_x &= \frac{\hbar k_x}{m} + \frac{\alpha}{\hbar}\sigma_y = i\frac{\hbar}{m}(a^\dagger - a)/(\sqrt{2}l_B) + \frac{\alpha}{\hbar}\sigma_y, \\ v_y &= \frac{\hbar(k_y + eA_y/\hbar)}{m} - \frac{\alpha}{\hbar}\sigma_x = -\frac{\alpha}{\hbar}\sigma_x + \frac{\hbar}{m}(a^\dagger + a)/(\sqrt{2}l_B). \end{aligned} \tag{18}$$

In Eq. (17) $1/(2\tau)$ is a small residual scattering rate. Working out the appropriate matrix elements gives for the longitudinal dynamic conductivity

$$\begin{aligned} \sigma_{xx}(\omega) = {} & \frac{-ie^2}{2\pi l_B^2} \sum_s \frac{f_0 - f_{1,s}}{E_{N=0} - E_{1,s}} Q_x(0,1,+,s)\langle 0|v_x|1,s\rangle\langle 1,s|v_x|0\rangle \\ & + \frac{-ie^2}{2\pi l_B^2} \sum_{N=1,s,s'} \frac{f_{N,s} - f_{N+1,s'}}{E_{N,s} - E_{N+1,s'}} Q_x(N,N+1,s,s')\langle N,s|v_x|N+1,s'\rangle\langle N+1,s'|v_x|N,s\rangle \end{aligned} \tag{19}$$

with $f_{N,s}$ the Fermi-Dirac distribution function given by $1/(e^{\beta(\omega-\mu)} + 1)$ with β the inverse temperature T and μ the chemical potential. The transverse dynamic Hall conductivity

$$\begin{aligned} \sigma_{xy}(\omega) = {} & \frac{-e^2}{2\pi l_B^2} \sum_s \frac{f_0 - f_{1,s}}{E_{N=0} - E_{1,s}} Q_y(0,1,+,s)\langle 0|v_x|1,s\rangle\langle 1,s|v_x|0\rangle \\ & + \frac{-e^2}{2\pi l_B^2} \sum_{N=1,s,s'} \frac{f_{N,s} - f_{N+1,s'}}{E_{N,s} - E_{N+1,s'}} Q_y(N,N+1,s,s') \times \langle N,s|v_x|N+1,s'\rangle\langle N+1,s'|v_x|N,s\rangle, \end{aligned} \tag{20}$$

where

$$\begin{pmatrix} Q_x(N,N',s,s') \\ Q_y(N,N',s,s') \end{pmatrix} = \frac{1}{\omega + E_{N,s} - E_{N',s'} + i/(2\tau)} \pm \frac{1}{\omega + E_{N',s'} - E_{N,s} + i/(2\tau)}. \tag{21}$$

Here we will be interested in the absorptive part of the conductivity, namely $\mathrm{Re}\,\sigma_{xx}$ and $\mathrm{Im}\,\sigma_{xy}$, which can be written in the form

$$\begin{aligned} \begin{pmatrix} \mathrm{Re}\,\sigma_{xx}(\omega) \\ \mathrm{Im}\,\sigma_{xy}(\omega) \end{pmatrix} &= \mp\frac{e^2}{2\hbar}\sum_s \frac{f_0 - f_{1,s}}{E_{N=0} - E_{1,s}}\frac{F(0,s)}{H(0,s)}E_0[\delta(\hbar\omega - E_0H(0,s)) \pm \delta(\hbar\omega + E_0H(0,s)] \\ &\quad \mp\frac{e^2}{2\hbar}\sum_{N=1,s,s'}(f_{N,s} - f_{N+1,s'})\frac{F(N,s,s')}{H(N,s,s')}E_0[\delta(\hbar\omega - E_0H(N,s,s')) \pm \delta(\hbar\omega + E_0H(N,s,s')], \end{aligned} \tag{22}$$

where the delta function $\delta(x)$ conserves energy in the optical absorption process and we have defined

$$H(N,s,s') = -1 + s\sqrt{1/4 + 2NP} - s'\sqrt{1/4 + 2(N+1)P} \tag{23}$$

and

$$F(N,s,s') = \left(\frac{\sqrt{N}}{\sqrt{2}}C^*_{\uparrow,N+1,s'}C_{\uparrow,N,s} + \frac{\sqrt{N+1}}{\sqrt{2}}C^*_{\downarrow,N+1,s'}C_{\downarrow,N,s} - \sqrt{P}C^*_{\uparrow,N+1,s'}C_{\downarrow,N,s}\right)^2; \tag{24}$$

for $N \neq 0$ and for $N = 0$

$$H(0,s) = -1/2 - s\sqrt{1/4 + 2P}, \tag{25}$$

$$F(0,s) = \left(\frac{1}{\sqrt{2}}C_{\downarrow,1,s} - \sqrt{P}C_{\uparrow,1,s}\right)^2. \tag{26}$$

In Fig. 3 we show results for the Landau level energies obtained from Eq. (7) for the specific case of Bi_2Te_3 with $m/m_e = 0.09$ as a function of magnetic field B in Tesla. The solid lines are for positive N's as well as $N = 0$ while the dotted are for negative N's. The energies of the positive branch levels are not as strongly modified by the quadratic Schrödinger term in Eq. (1) than are the energies of the negative branch. For the pure Dirac case there would be mirror symmetry between positive and negative levels and they would all scale as the square root of the magnetic field B. Now the positive N levels show small deviations from $\sqrt{B}$ law while the negative N levels begin to bend over upward as B increases, and can even cross the $E = 0$ axis at 40 T for the larger values of N shown. The solid black curve for $N = 0$ is linear in B and goes to zero at $B = 0$. For pure Dirac this level would remain at zero for all values of magnetic field. The lack of perfect mirror symmetry between positive and negative branches of the spectrum has important implications for the peaks seen in both $\mathrm{Re}\,\sigma_{xx}(\omega)$ and $\mathrm{Im}\,\sigma_{xy}(\omega)$ as a function of ω. This is illustrated in Fig. 4 which has four frames. The upper two are for a value of chemical potential which falls between $N = 0$ and $N = 1$ Landau levels (LL), while in the two lower frames the chemical potential μ falls between the $N = 1$ and $N = 2$ LL. In all cases $\Gamma = 1/(2\tau)$ in Eqs. (19) and (20) was set to $15K$ and the magnetic field at 1 T. The frames come in pairs; the top panel includes a finite mass for the quadratic term in the Hamiltonian (1) $m/m_e = 0.09$ while the lower panel of each pair is for comparison and has $m/m_e = \infty$ (the pure Dirac limit). Also, the solid continuous black curve is for the real part of the longitudinal conductivity $\mathrm{Re}\,\sigma_{xx}(\omega)$ vs ω and the dotted red curve for the imaginary part of the Hall conductivity $\mathrm{Im}\,\sigma_{xy}(\omega)$ vs ω. Starting with the upper two frames, we note first that including the quadratic term in the dispersion relation has split the peaks in the solid curves into two except for the first one. This feature can be traced directly to the energy level scheme of Fig. 3 and the lack of perfect symmetry between positive and negative branches. The arrows in the left hand lower frame connect energy levels for the allowed optical transitions (the chemical potential $\mu = 50\,K$ is shown as the horizontal black dashed line which falls slightly above

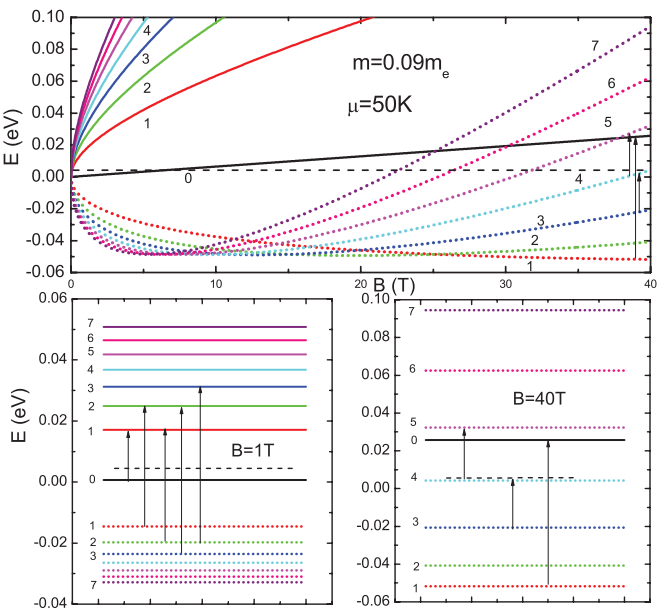

FIG. 3. (Color online) The top panel gives the energies $E_{N,s}$ of the Landau levels for various values of N (as labeled) as a function of the magnetic field B. The conduction band levels are solid curves and the valence band levels are dotted curves. Here the quadratic mass term has $m = 0.09m_e$. The horizontal dashed line is the chemical potential level $\mu = 50K$. In the two lower panels we show a few allowed optical transitions indicated by arrows with chemical potential shown by the horizontal black dashed line. The left panel is for B = 1 Tesla and the right for $B = 40$ T. Here $\alpha/\hbar = 4.3 \times 10^5$ m/s, representative of Bi_2Te_3. For Bi_2Se_3 it is instead 5×10^5 m/s.

the solid black line associated with the $N = 0$ level). Note that the zeroth Landau level is not quite at $E = 0$ because B is finite (1 T). The optical selection rules allow N to change by only 1. In addition one needs to go from occupied to unoccupied states through the absorption of the photon. The first peak in $\mathrm{Re}\,\sigma_{xx}(\omega)$ and $\mathrm{Im}\,\sigma_{xy}(\omega)$ come from the transition indicated by the shortest arrow on the left from $N = 0$ to $N = 1$. There is only one such arrow and consequently only one peak in the conductivity. However, for the second peak two arrows contribute, that from $N = 1$ (negative side) to $N = 2$ (positive side) and from $N = 2$ (negative side) to $N = 1$ (positive side). For the pure Dirac case these two arrows would have exactly the same length and there is only one peak in the conductivity, as we see in the lower frame of Fig. 4 for μ

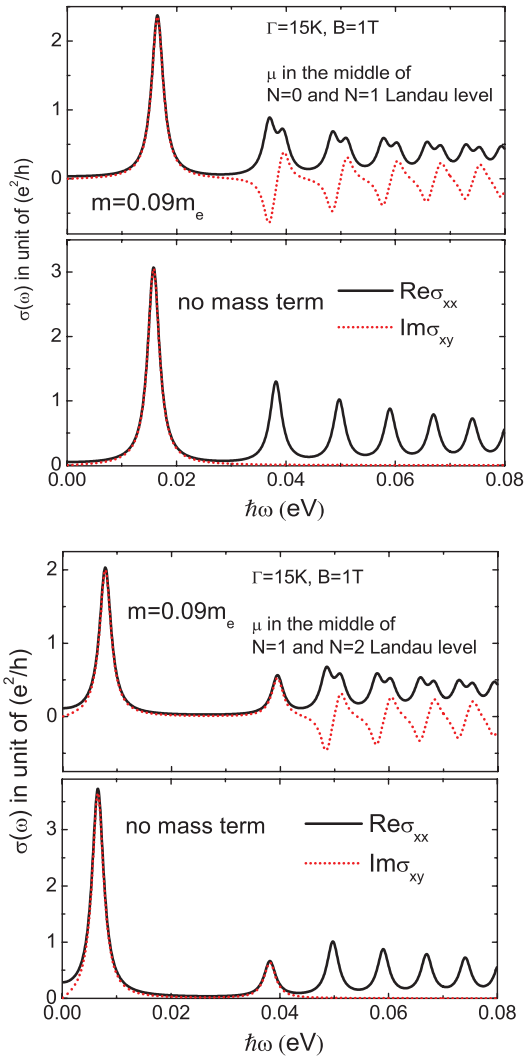

FIG. 4. (Color online) The real part of the longitudinal optical conductivity $\sigma_{xx}(\omega)$ (solid black curve) compared with the imaginary part of the transverse Hall conductivity $\sigma_{xy}(\omega)$ (dotted red curve) in units of e^2/h as a function of photon energy $\hbar\omega$ in eV. The electron mass term has $m = 0.09m_e$, the residual scattering rate is $\Gamma = 15K$, and the magnetic field $B = 1$ T. The top two frames are for chemical potential falling between $N = 0$ and $N = 1$ Landau levels while in the lower two frames it falls between $N = 1$ and $N = 2$. In each case we show first results for finite m and below for $m = \infty$ (pure Dirac) which is included for comparison. Here $\alpha/\hbar = 4.3 \times 10^5$ m/s.

between $N = 0$ and $N = 1$. But when there is a quadratic term in Eq. (1) the symmetry between positive and negative branches is no longer observed, and the two arrows in question are of slightly different length. This line is split into two peaks in the conductivity. The amount of splitting reflects directly the difference in the absolute value of the energy between positive and negative branches for the same N. Here we have used $m/m_e = 0.09$ for Bi_2Te_3. For smaller values of m the observed splitting would increase for fixed Dirac spectrum (α). The consequences of this mismatch between energies of positive and negative energy branches is even more striking for the Hall than it is for the longitudinal conductivity. The red dotted curve in the upper frame shows a first negative oscillation and then a positive peak. For the pure Dirac case these two peaks would have the same energy and hence cancel out perfectly as we see in the second frame of Fig. 4. In that case only the first peak remains in the Hall conductivity, all higher peaks are missing due to the cancellation just described. Turning next to the second set of two frames of Fig. 4 we see a similar pattern but with significant differences that need to be commented upon. In this case we have increased the value of the chemical potential so that it falls between the positive $N = 1$ and $N = 2$ Landau levels. Firstly note that the first peak has shifted to lower energy while all others stay at the same energies as in the upper two frames, but the intensity of the second peak has been reduced by a factor of 2 for the pure Dirac case. Secondly, in the mixed Schrödinger-Dirac case the first negative oscillation in Hall conductivity is absent, as is the lower split peak in the longitudinal conductivity. These features are easily understood with the help of the energy level diagram, left lower frame of Fig. 3. Moving the chemical potential level (dashed line) to fall between $N = 1$ and $N = 2$ we see that the transition with the shortest arrow is no longer allowed by the optical selection rule. The second arrow from $N = 1$ (negative branch) to $N = 2$ (positive branch) remains a possible optical transition while the transition from $N = 2$ (negative branch) to $N = 1$ (positive branch) is Pauli blocked and is no longer possible. The final state is already occupied. There is only one arrow that can contribute and half the line is lost so the second peak is no longer split. This is one of our important results.

So far we have described in relation to Fig. 4 only the interband transitions between negative and positive branches. But the optical selection rule also allows intraband transitions between N and $N + 1$ of the same branch. To understand how it is that the lowest peak in both $\mathrm{Re}\,\sigma_{xx}(\omega)$ and $\mathrm{Im}\,\sigma_{xy}(\omega)$ has shifted to lower energies in the two lower frames of Fig. 4, we need to include intraband transitions. Returning to the level diagram of Fig. 3, lower left frame, we can see that for μ between $N = 1$ and $N = 2$ levels an optical transition from 1 (occupied) to 2 (unoccupied) is now possible, and this gives the first peak (seen in our Fig. 4 two lower frames) which is a intraband peak and replaces the first interband peak (in the upper two frames) which is no longer possible. These results are based on the simplest Hamiltonian (1) which includes only a Schrodinger quadratic-in-momentum term and a Dirac linear-in-k contribution. Recently Fu[29] found that to understand the ARPES data in Bi_2Te_3 a cubic hexagonal correction needs to be added to the Hamiltonian. The role of hexagonal warping played in optics was further discussed

in Ref. 10. It was found to change the constant universal background provided by the interband optical transitions to a sloped background which increases with increasing photon energy. The application of a magnetic field introduces Landau level (LL) oscillations based on this background. Consequently, as a first approximation, we expect that including hexagonal warping with a magnetic field would lead to LL oscillations which would average out at higher energies to a sloped rather than a constant background.

The peak structure just described for $\mathrm{Re}\,\sigma_{xx}(\omega)$ and $\mathrm{Im}\,\sigma_{xy}(\omega)$ has important implication for the behavior of the conductivity for right and left handedness polarized light defined as $\sigma_{\pm}(\omega) \equiv \sigma_{xx}(\omega) \pm i\sigma_{xy}(\omega)$. This is shown in Fig. 5 which has a direct correspondence to the data presented in Fig. 4 and which also has four frames. The top two are for μ between $N = 0$ and $N = 1$ LL and the lower two for μ between $N = 1$ and $N = 2$ LL. The solid black curve is $\mathrm{Re}\,\sigma_{+}(\omega)$ and the dotted red is $\mathrm{Re}\,\sigma_{-}(\omega)$. Note that there are no split peaks in these quantities but striking differences between the Schrödinger plus Dirac case and pure Dirac (lower frame of each pair) remain. For pure Dirac, $\mathrm{Re}\,\sigma_{-}(\omega)$ (red dotted curve) has a single peak corresponding to the lowest energy peak of Fig. 4. This peak is missing in $\mathrm{Re}\,\sigma_{+}(\omega)$ which, however, has all the other peaks seen in Fig. 4. For the mixed Schrödinger plus Dirac case the situation is similar with one important difference. The higher energy peaks remain in $\mathrm{Re}\,\sigma_{xx}(\omega)$ (red dotted curve) but they are displaced in energy with respect to those in the solid black curve. These differences between pure Dirac and the case with the existence of a subdominant Schrödinger part to the Hamiltonian [Eq. (1)] could be used to estimate the magnitude of this second contribution.

So far we have considered only the case of $B = 1$ T and have found differences with the pure Dirac case. These differences can be made much more dramatic by increasing the magnitude of the external magnetic field, as we show in Fig. 6 for magnetic field $B = 40$ T. As we see in the top frame of Fig. 3 for the Landau level energies, the $N = 0$ level has now moved to $E_0 \simeq 0.025$ eV. While for $N = 1,2,3$ the valence band energies remain negative, they have moved to positive values for $N = 4$ and above. In the right hand lower frame of Fig. 3 we show these various levels as well as the chemical potential (black dashed curve) which we take to fall just above the $N = 4$ level of the negative branch (dotted cyan lines). All other levels fall outside the energy range shown in the figure. Because we are at finite temperature, the possible optical transitions are shown as arrows from 4 to 5, from 3 to 4, and from 1 to 0. The first two are close in energy and give a split peak in the top frame of Fig. 6 for $\mathrm{Re}\,\sigma_{xx}(\omega)$ with mass term included. The lower peak in the split pair, which is due to the 3 to 4 transition, will disappear at zero temperature as this transition is now Pauli blocked. The long arrow gives the second single peak at about 0.07 eV in the black curve. This transition also contributes to the imaginary part of the Hall conductivity (dotted red) which shows a negative peak. It also displays the same lower energy split peak as does the longitudinal conductivity. Consequently the left circular polarization conductivity $\mathrm{Re}\,\sigma_{-}(\omega)$ (red dotted) shows a low energy split peak of twice the amplitude of its value in $\mathrm{Re}\,\sigma_{xx}(\omega)$ and no other peak, while the right circular polarization conductivity $\mathrm{Re}\,\sigma_{+}(\omega)$ (black solid) shows a single positive peak at about 0.07 eV. This is to be contrasted with the pure Dirac case shown in the lower frame of each pair of diagrams. In that case there is a single line in the energy range shown. It is present in $\mathrm{Re}\,\sigma_{xx}(\omega)$ (black solid) and in $\mathrm{Im}\,\sigma_{xy}(\omega)$ (dotted red) with the same amplitude as well as in $\mathrm{Re}\,\sigma_{-}(\omega)$ (dotted red) with twice the amplitude. It does not appear in $\mathrm{Re}\,\sigma_{+}(\omega)$.

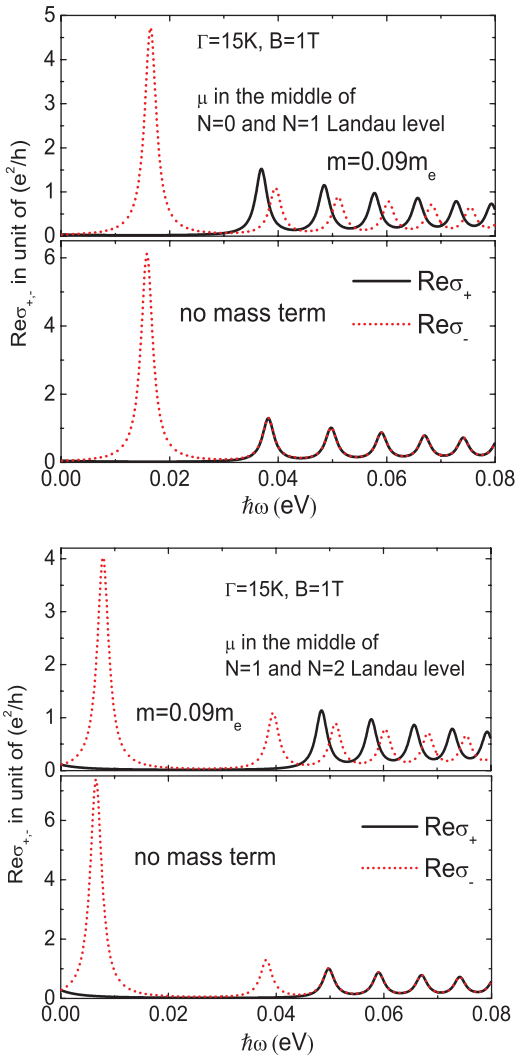

FIG. 5. (Color online) The real part of right (+) and left handed circularly polarized optical conductivity $\sigma_{\pm}(\omega)$ in units of e^2/h as a function of photon energy $\hbar\omega$ in eV. In all panels the residual scattering rate $\Gamma = 15K$ and the magnitude of the magnetic field is set at $B = 1$ T. The top two panels are for a case when the chemical potential falls between $N = 0$ and $N = 1$ Landau levels and for the bottom two it falls between N = 1 and N = 2. In all cases solid black is for right hand polarization and the dotted red for left polarization. The panels come in pairs; in the top frame the quadratic term in the Hamiltonian has mass $m = 0.09m_e$, while $m = \infty$ (pure Dirac) for the bottom frame of each pair,for comparison. Here $\alpha/\hbar = 4.3 \times 10^5$ m/s.

IV. SEMICLASSICAL LIMIT

The semiclassical limit of the magneto-conductivity is obtained when the chemical potential μ is much larger than

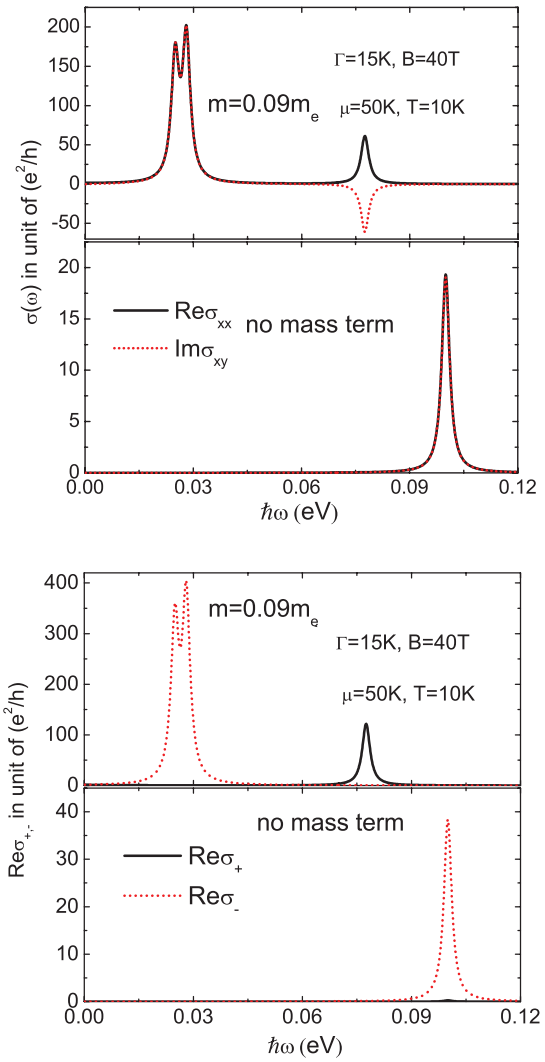

FIG. 6. (Color online) The top pair of frames give the real part (imaginary part) of the longitudinal [transverse Hall] conductivity $\mathrm{Re}\,\sigma_{xx}(\omega)$, solid black [$\mathrm{Im}\,\sigma_{xy}(\omega)$, red dotted] in units of e^2/h as a function of photon energy $\hbar\omega$ in eV. The top panel has a finite quadratic piece in its dispersion curve with mass $m = 0.09m_e$ while the bottom panel has $m = \infty$. In both cases the residual scattering rate $\Gamma = 15K$ the chemical potential $\mu = 50K$, the temperature $T =$ 10 K, and the magnetic field is set at $B = 40$ T. The bottom two frames are for the same parameter set and the notation is the same. What is plotted, however, is the right σ_+ solid black and left σ_- dotted red circularly polarized conductivity. Here $\alpha/\hbar = 4.3 \times 10^5$ m/s.

the magnetic energy. In this case for $\mu > 0$ only intraband transitions are involved, as we are interested in the cyclotron resonance energy range which is much less than μ. This involves large values of N. Let μ fall between the Nth and $(N+1)$th Landau levels. So

$$\mu = NE_0 + \sqrt{2NE_1^2 + (E_0/2)^2} \simeq NE_0 + \sqrt{2N}E_1, \quad (27)$$

and the energy of the optical transition from N to $N+1$ is given by

$$\hbar\omega_c \simeq E_{N+1} - E_N, \quad (28)$$

which is the semiclassical cyclotron frequency. We can solve Eq. (27) to get N in terms of μ and obtain

$$\sqrt{N} = \frac{E_1}{\sqrt{2}E_0}\left[\sqrt{1 + 2\mu E_0/E_1^2} - 1\right] \quad (29)$$

and so

$$\hbar\omega_c = \frac{\hbar eBv_F^2}{\mu}\frac{\sqrt{1 + 2\mu\hbar^2/m\alpha^2}\left[\sqrt{1 + 2\mu\hbar^2/m\alpha^2} + 1\right]}{2}. \quad (30)$$

For $m \to \infty$ we have the well known results for the pure Dirac case

$$\hbar\omega_c = \frac{eBv_F^2\hbar}{\mu}. \quad (31)$$

The first correction for m large but not infinite is

$$\hbar\omega_c = \frac{eBv_F^2\hbar}{\mu}\left[1 + \frac{3}{2}\mu/\left(mv_F^2\right) - \frac{1}{4}\mu^2/\left(mv_F^2\right)^2\right]. \quad (32)$$

The pure Schrödinger case is obtained as $\alpha \to 0$ which gives

$$\hbar\omega_c = \frac{\hbar eB}{m}, \quad (33)$$

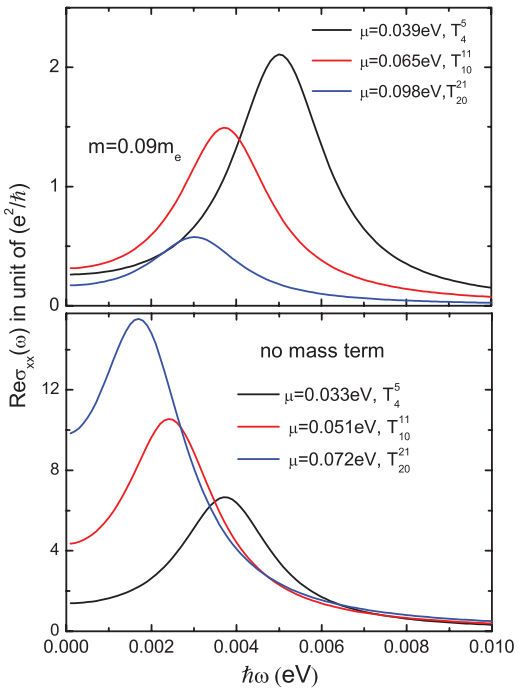

FIG. 7. (Color online) The semiclassical limit of the real part of the longitudinal conductivity $\mathrm{Re}\,\sigma_{xx}(\omega)$ in units of e^2/h as a function of photon energy $\hbar\omega$ in eV. The top and bottom frames give results when $m = 0.09m_e$ and $m = \infty$ (no quadratic mass term) respectively. Also identified are the optical transition between Landau levels that are involved (see lower right panel of Fig. 3) and the corresponding values of chemical potential μ. The three cases considered are color coded. Note that for $m = \infty$ (lower panel) the amplitude of the conductivity at the cyclotron frequency increases monotonically as the chemical potential increases, while instead it decreases when $m = 0.09m_e$. Here $\alpha/\hbar = 4.3 \times 10^5$ m/s.

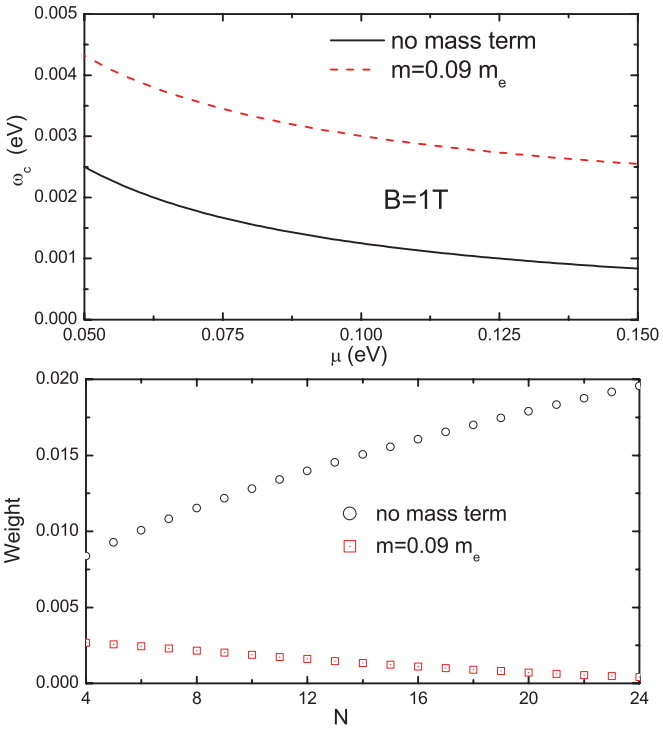

FIG. 8. (Color online) The top panel gives the semiclassical cyclotron frequency as a function of chemical potential μ and the bottom panel gives the optical spectral weight under the Nth line for $m = 0.09m_e$ (open square) compared with its value for pure Dirac (open circle). Here $\alpha/\hbar = 4.3 \times 10^5$ m/s.

and the lowest order correction for α small but not zero is

$$\hbar\omega_c = \frac{\hbar eB}{m}[1 + \sqrt{m\alpha^2/2\mu\hbar^2} + m\alpha^2/2\mu\hbar^2]. \quad (34)$$

For Bi_2Te_3 we estimate $m\alpha^2/(2\hbar^2) = 0.048$ eV and $eBv_F^2\hbar = 1.2 \times 10^{-4}$ $(\text{eV})^2$ and for Bi_2Se_3 we have 0.115 eV and 1.6×10^{-4} $(\text{eV})^2$ respectively. For the first case we show in the upper frame of Fig. 8 the cyclotron energy as a function of chemical potential (red dashed curve) which we compare with pure Dirac (black solid curve). Both show similar variation with μ (inverse μ law) but the two curves are significantly displaced from each other for the case $m/m_e = 0.09$. For smaller values of the mass m the effect of a subdominant Schrödinger contribution to the cyclotron frequency will be even larger.

The real part of the longitudinal conductivity $\text{Re}\,\sigma_{xx}(\omega)$ vs ω in units of $e^2/\hbar$ in the semiclassical regime is shown in Fig. 7. The top frame is for the parameters that we have associated with Bi_2Te_3 with $m/m_e = 0.09$, while the bottom frame results when the Schrödinger piece of the energy [Eq. (1)] is dropped, for comparison. The values of chemical potential used and the optical transitions involved are labeled and color coded in the figure. Not only is the value of the central frequency (ω_c) giving the peak in these line-shapes different when m/m_e is finite as compared with its value when m/m_e is infinite, but also the line-shapes themselves are quite different. As ω_c increases the optical spectral weight [area under the curve for $\text{Re}\,\sigma_{xx}(\omega)$] decreases in the $m = \infty$ case while it increases for $m/m_e = 0.09$. This is illustrated further in the lower frame of Fig. 8 where we plot the spectral weight as a function of N with (open squares) and without (open circles) a mass term. Note that this quantity is related to the ratio $F(N,+,+)E_0/H(N,+,+)$ which appears in Eq. (22) with H and F given by Eqs. (23) and (24) respectively. We see that including a small mass term has a profound effect on this spectral weight, which is another important result of this analysis.

V. SUMMARY AND CONCLUSIONS

We have studied how adding a small subdominant quadratic-in-momentum term to a dominant Dirac dispersion modifies the magneto-conductivity when Landau levels are formed in a topological insulator by application of a magnetic field B. In such a case the energies of the Landau levels in conduction and valence band no longer mirror each other. This means that interband optical transitions from level N in the valence band to $N+1$ in the conduction band no longer have the same energy as those from $N+1$ to N, and this splits the corresponding absorption line for the real part of the longitudinal conductivity into two, each carrying the identical optical spectral weight. The energy of the splitting is related to the mismatch in energy levels between conduction and valence bands. A similar splitting is found for the imaginary part of the Hall conductivity. However, for the absorption of circularly polarized light, single-peak structures are recovered but in this case there is a shift in the energy position of the lines between right and left polarization in contrast to what is found when the mass term in the electron dispersion curves is zero for pure Dirac. The semiclassical limit is also affected by the presence of a subdominant quadratic term. This significantly shifts the value of the cyclotron frequency away from its pure Dirac value of $eBv_F^2\hbar/\mu$ and introduces a more complicated dependence on chemical potential given in Eq. (30). The lineshape associated with the cyclotron resonance is significantly changed. The optical spectral weight under these curves is found to decrease with increasing value of the chemical potential rather than increase as would be the case in a pure relativistic Dirac system.

ACKNOWLEDGMENTS

This work was supported by the Natural Sciences and Engineering Research Council of Canada (NSERC) and the Canadian Institute for Advanced Research (CIFAR), and in part by the Perimeter Institute for Theoretical Physics, which is supported by the Government of Canada through Industry Canada and by the Province of Ontario through the Ministry of Economic Development and Innovation.

*lizhou@univmail.cis.mcmaster.ca
†carbotte@univmail.cis.mcmaster.ca

[1] M. Z. Hasan and C. L. Kane, Rev. Mod. Phys. **82**, 3045 (2010).
[2] X.-L. Qi and S.-C. Zhang, Rev. Mod. Phys. **83**, 1057 (2011).
[3] D. Hsieh *et al.*, Nature (London) **452**, 970 (2008).
[4] Y. L. Chen, J. G. Analytis *et al.*, Science **325**, 178 (2009).
[5] D. Hsieh *et al.*, Nature (London) **460**, 1101 (2009).
[6] C. Jozwiak, X. L. Chen *et al.*, Phys. Rev. B **84**, 165113 (2011).

[7]S.-Y. Xu, X. Xia *et al.*, Science **332**, 560 (2011).
[8]X.-L. Qi and S.-C. Zhang, Phys. Today **63**, 33 (2010).
[9]J. N. Hancock, J. L. M. van Mechelen, A. B. Kuzmenko, D. van der Marel, C. Brüne, E. G. Novik, G. V. Astakhov, H. Buhmann, and L. W. Molenkamp, Phys. Rev. Lett. **107**, 136803 (2011).
[10]Zhou Li and J. P. Carbotte, Phys. Rev. B **87**, 155416 (2013).
[11]V. P. Gusynin, S. G. Sharapov, and J. P. Carbotte, Phys. Rev. Lett. **98**, 157402 (2007).
[12]V. P. Gusynin, S. G. Sharapov, and J. P. Carbotte, New J. Phys. **11**, 095013 (2009).
[13]Z. Li, E. A. Henniksen *et al.*, Nat. Phys. **4**, 532 (2008).
[14]M. Orlita and M. Potemski, Semicond. Sci. Technol. **25**, 063001 (2010).
[15]I. Crasee, J. Levallois *et al.*, Nat. Phys. **7**, 48 (2011).
[16]E. J. Nicol and J. P. Carbotte, Phys. Rev. B **77**, 155409 (2008).
[17]T. Stauber and N. M. R. Peres, J. Phys.: Condens. Matter **20**, 055002 (2008).
[18]Zhou Li and J. P. Carbotte, Phys. Rev. B **86**, 205425 (2012).
[19]Zhou Li and J. P. Carbotte, Physica B **421**, 97 (2013).
[20]L. Stille, C. J. Tabert, and E. J. Nicol, Phys. Rev. B **86**, 195405 (2012).
[21]V. P. Gusynin, S. G. Sharapov, and J. P. Carbotte, J. Phys.: Condens. Matter **19**, 026222 (2007).
[22]A. Pound, J. P. Carbotte, and E. J. Nicol, Phys. Rev. B **85**, 125422 (2012).
[23]M. L. Sadowski, G. Martinez, M. Potemski, C. Berger, and W. A. de Heer, Phys. Rev. Lett. **97**, 266405 (2006).
[24]Z. Jiang, E. A. Henriksen, L. C. Tung, Y.-J. Wang, M. E. Schwartz, M. Y. Han, P. Kim, and H. L. Stormer, Phys. Rev. Lett. **98**, 197403 (2007).
[25]C. J. Tabert and E. J. Nicol, Phys. Rev. Lett. **110**, 197402 (2013).
[26]A. A. Schafgans, K. W. Post, A. A. Taskin, Y. Ando, X.-L. Qi, B. C. Chapler, and D. N. Basov, Phys. Rev. B **85**, 195440 (2012).
[27]A. A. Taskin and Y. Ando, Phys. Rev. B **84**, 035301 (2011).
[28]C.-X. Liu, X.-L. Qi, H. J. Zhang, X. Dai, Z. Fang, and S.-C. Zhang, Phys. Rev. B **82**, 045122 (2010).
[29]L. Fu, Phys. Rev. Lett. **103**, 266801 (2009).